



FRactal Spectroscopy by Noise-Free Stochastic Multiresonance at Higher Harmonics

A. KRAWIECKI, S. MATYJAŚKIEWICZ* and J. A. HOLYST

*Faculty of Physics, Warsaw University of Technology,
Koszykowa 75, PL-00-662 Warsaw, Poland*

**Institute of Physics, Humboldt University at Berlin,
Invalidenstraße 110, D-10115 Berlin, Germany*

K. KACPERSKI

*Department of Physics, Queen Mary College,
University of London, Mile End Road, London E1 4NS, UK*

Received April 15, 2002; Revised October 11, 2002

Noise-free stochastic resonance is investigated in two chaotic maps with periodically modulated control parameter close to a boundary crisis: the Hénon map and the kicked spin model. Response of the maps to the periodic signal at the fundamental frequency and its higher harmonics is examined. The systems show noise-free stochastic multiresonance, i.e. multiple maxima of the signal-to-noise ratio at the fundamental frequency as a function of the control parameter. The maxima are directly related to the fractal structure of the attractors and basins of attraction colliding at the crisis point. The signal-to-noise ratios at higher harmonics show more maxima, as well as dips where the signal-to-noise ratio is zero. This opens a way to use noise-free stochastic resonance to probe the fractal structure of colliding sets by a method which can be called “fractal spectroscopy”. Using stochastic resonance at higher harmonics can reveal smaller details of the fractal structures, but the interpretation of results becomes more difficult. Quantitative theory based on a model of a colliding fractal attractor and a fractal basin of attraction is derived which agrees with numerical results for the signal-to-noise ratio at the fundamental frequency and at the first two harmonics, quantitatively for the Hénon map, and qualitatively for the kicked spin model. It is also argued that the maps under study belong to a more general class of threshold-crossing stochastic resonators with a modulated control parameter, and qualitative discussion of conditions under which stochastic multiresonance appears in such systems is given.

Keywords: Stochastic resonance; deterministic chaos; fractals; crisis.

1. Introduction

Stochastic resonance (SR) is a phenomenon occurring in systems driven by a combination of a periodic signal and random noise, such that the periodic component present in a suitably defined output signal becomes most pronounced for optimum, nonzero input noise intensity [Benzi *et al.*, 1981] (for review see [Jung, 1993; Moss, 1994; Moss

et al., 1994; Wiesenfeld & Moss, 1995; Gammaitoni *et al.*, 1998; Anishchenko *et al.*, 1999; Moss, 2000]). A related phenomenon is noise-free (deterministic) SR which appears in periodically driven chaotic systems without external random forcing, in which the internal chaotic dynamics can be tuned, by varying the control parameter, to achieve the maximization of the periodic component of the output

signal. Noise-free SR was demonstrated, e.g. in periodically driven chaotic maps [Anishchenko *et al.*, 1993; Nicolis *et al.*, 1993; Krawiecki, 1997; Sinha & Chakrabarti, 1998; Horita *et al.*, 1999; Ginzburg & Pustovoit, 1999; Sinha, 1999; Zhou & Lai, 1999a, 1999b; Matyjaśkiewicz *et al.*, 2001; Krawiecki *et al.*, 2001], in chaotic systems with continuous time [Carroll & Peccora, 1993; Anishchenko *et al.*, 1994; Crisanti *et al.*, 1994; Kovaleva & Simiu, 2000; Arai *et al.*, 2002], in simulations of models of coupled biological neurons [Wang & Wang, 1997; Nishimura *et al.*, 2000; Yuqing *et al.*, 2000], in experiments with chaotic spin-wave dynamics [Reibold *et al.*, 1997] and with chaotic lasers [Pisarchik & Corbalán, 1998; Chizhevsky *et al.*, 2000]. Characterization of SR is usually based on the power spectral density (PSD) of the output signal, which consists of peaks at the frequency of the input periodic signal (the fundamental frequency), and, possibly, its higher harmonics, superimposed on a broadband noise background. The strength of the periodic component of the output signal can be expressed as the signal-to-noise ratio (SNR) at the fundamental frequency, defined as the ratio of the output power at the fundamental frequency to the noise power in the vicinity of this frequency. The hallmarks of SR and noise-free SR are that the SNR has a maximum as a function of the input noise intensity or the control parameter, respectively. In systems with SR, investigation of the output signal power at higher harmonics of the fundamental frequency is also of considerable interest [Bartussek *et al.*, 1994; Shneidman *et al.*, 1994; Bartussek *et al.*, 1995; Jung & Talkner, 1995; Bulsara *et al.*, 1996; Grifoni & Hänggi, 1996; Grigorenko *et al.*, 1997; Krawiecki, 1997; Loerincz *et al.*, 1999]. To characterize the system response at higher harmonics the respective SNR can be used, defined as the ratio of the output power at the higher harmonic to the noise power in its vicinity. The SNR at higher harmonics as a function of the input noise intensity typically shows two or more maxima separated by dips, where the SNR is zero. This behavior was observed, and explained theoretically, in generic bistable [Bartussek *et al.*, 1994; Jung & Talkner, 1995; Bulsara *et al.*, 1996], monostable [Grigorenko *et al.*, 1997] and threshold-crossing (TC) [Loerincz *et al.*, 1999] models of SR, as well as in quantum [Grifoni & Hänggi, 1996] and noise-free SR [Krawiecki, 1997]. Recently it has been shown that in certain systems the SNR at the fundamental frequency can exhibit

several, or even infinitely many, maxima as the noise intensity [Jung & Hänggi, 1991; Vilar & Rubí, 1997, 1999] or the control parameter in a chaotic system [Matyjaśkiewicz *et al.*, 2001; Krawiecki *et al.*, 2001] are varied, and these phenomena were given names stochastic multiresonance (SMR) and noise-free SMR, respectively. Several experimental observations of SMR or similar phenomena have been reported [Hou *et al.*, 1999; Tsindlekht *et al.*, 2000; Shiau & Néda, 2001; Zhang & Xin, 2001]. The purpose of this paper is to review the results on the noise-free SMR at the fundamental frequency in periodically driven chaotic systems, and to extend the investigation to study their response at higher harmonics of the fundamental frequency.

As models of systems with noise-free SR discrete-time chaotic maps in the vicinity of boundary crises [Grebogi *et al.*, 1986; Grebogi *et al.*, 1987] can be used. If the control parameter is below the crisis point, such maps have at least one chaotic attractor and associated basin of attraction (henceforth referred to as precritical attractor and basin of attraction, respectively). At the crisis point the attractor collides with the border of its basin of attraction. With the parameter increased further, it turns into a chaotic saddle and the phase trajectory starts leaking out, eventually escaping from its neighborhood. A kind of reinjection mechanism, either natural (e.g. in symmetric attractor merging crisis, or interior crisis), or arbitrarily introduced, provides for an intermittent postcritical dynamics: consecutive escape events followed by returns on the chaotic saddle. Such systems can be described as TC systems [Wiesenfeld *et al.*, 1994; Gingl *et al.*, 1995; Chapeau-Blondeau, 1995; Chapeau-Blondeau & Godivier, 1997], with the escape events playing a role of TC events. If a weak periodic in time signal is added to the control parameter, a maximum of the SNR at the fundamental frequency, and thus noise-free SR, is observed for the optimum value of the control parameter in these model systems. If the escape probability above the crisis point increases monotonically with the control parameter, only one maximum of the SNR occurs, in analogy with SR in generic TC systems with external noise. In contrast, the models we study in this paper are two-dimensional maps, in which the precritical chaotic attractors and, possibly, their basins of attraction are fractal sets. As a result, the escape probability does not increase smoothly and monotonically with the control parameter; in

contrast, noticeable oscillations are superimposed on this general trend. For small enough amplitudes and low frequencies of the periodic signal these oscillations lead to multiple maxima of the SNR at the fundamental frequency as a function of the constant part of the control parameter, and thus to noise-free SMR [Matyjaśkiewicz *et al.*, 2001; Krawiecki *et al.*, 2001]. Here we extend the latter result to the case of the SNR at higher harmonics of the input signal, and show that even more maxima, separated by dips where the SNR is zero, are then observed. Thus the dependence of the SNR at higher harmonics on the control parameter becomes very complicated. Nevertheless, we are able to formulate analytic theory of the noise-free SMR in our model systems, based on simple models of fractal precritical attractors and their basins colliding at the crisis point. From this theory, significant features of the SNR at higher harmonics can be inferred, as it has been done previously for the SNR at the fundamental frequency [Matyjaśkiewicz *et al.*, 2001].

Our models with fractal-induced oscillations of the TC probability belong to a more general class of systems, in which the derivative of the TC probability with respect to some parameter is non-monotonic. If a small periodic signal is added to this parameter, such systems can exhibit SMR. Below we repeat the arguments of [Krawiecki *et al.*, 2001] leading to this general conclusion, and extend the discussion to address also SMR at higher harmonics. In the particular case of the model chaotic maps, this enables us to understand the origin of multiple maxima of the SNR at the fundamental frequency and its harmonics, as well as to find certain relationships between the SNR curves at consecutive harmonics.

The location and height of the maxima of the SNR in the model chaotic maps, at the fundamental frequency and at its higher harmonics, are directly related to the fractal structure and distribution of the invariant density on the precritical attractors and basins in the collision region at crisis. Large changes of the SNR with the rise of the control parameter correspond even to small changes of the part of the invariant density of the precritical attractor located outside its basin, and the SNR is very sensitive to tiny details of the fractal structures of these sets. This leads to the idea of using noise-free SR to probe the local (in the collision region) fractal structure of the attractors and basins

of attraction. More generally, this shows that easily observable quantities such as the SNR can be examined to obtain information on the local structure of the colliding sets, a method which can be called “fractal spectroscopy”.

2. The Model Systems and Numerical Results

2.1. The model chaotic maps

We begin with introduction of two-dimensional chaotic maps with crises, which are our model systems to study noise-free SMR. Chaotic crisis occurs if a chaotic attractor which exists for $q < q_c$, where q is the control parameter and q_c is the crisis threshold, at $q = q_c$ collides with the border of its basin of attraction [Grebogi *et al.*, 1986; Grebogi *et al.*, 1987]. For $q > q_c$ the attractor converts to a chaotic saddle and chaotic transients can be observed. During the transient the phase trajectory bounces around the saddle for some time, and then rapidly escapes to a distant part of the phase space. This happens when the phase trajectory pokes out the former basin of attraction into its former complementary set which we call a basin of escape. The mean escape time $\langle \tau(q) \rangle$ obeys the power scaling law

$$\langle \tau(q) \rangle = C(q - q_c)^{-\gamma}, \quad C = \text{const.} \quad (1)$$

Due to the fractal structures of the colliding chaotic saddle and, possibly, the basin of escape, in certain chaotic systems significant oscillations of $\langle \tau(q) \rangle$ can be superimposed on the general trend given by Eq. (1) [Kacperski & Hołyst, 1999a, 1999b]. The normal oscillations are connected with the subsequent branches of the fractal saddle entering, with the rise of q , the nonfractal basin of escape which results in the modulation of the slope of the curve $\langle \tau(q) \rangle$. The anomalous oscillations, including sections in which $\langle \tau(q) \rangle$ increases against the general trend, appear if the basin of escape has also a distinct fractal structure.

As a first example of a system with oscillations of the mean escape time the Hénon map will be considered: $x_{n+1} = p - x_n^2 - Jy_n$, $y_{n+1} = x_n$, where $J = 0.3$ and p is the control parameter. For $p < p_c = 2.12467245 \dots$ the map has two coexisting attractors: the chaotic precritical attractor, and another one at infinity, with complementary basins of attraction. At $p = p_c$ the chaotic precritical attractor is destroyed and for $p > p_c$, after the transient,

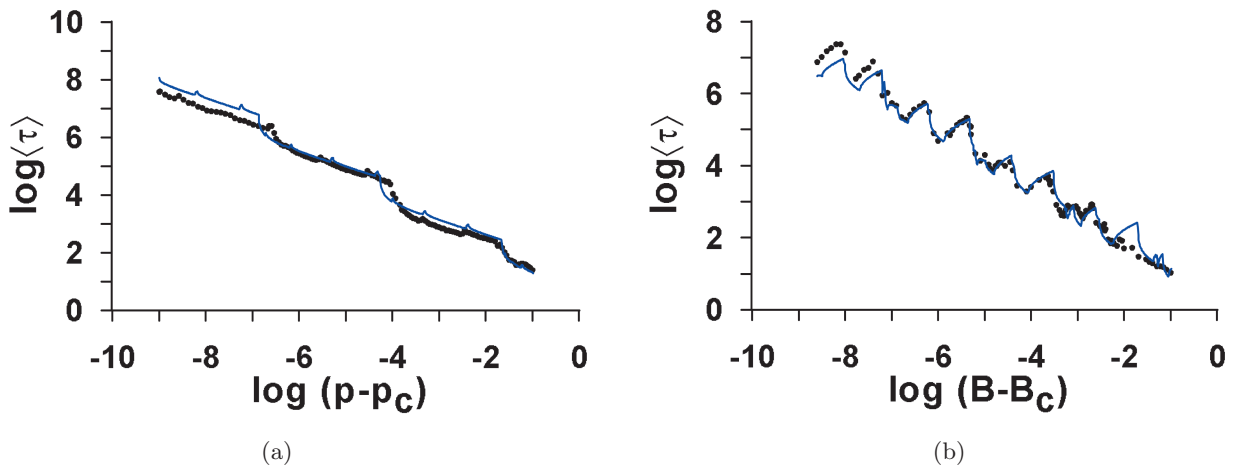


Fig. 1. Mean escape time $\langle \tau \rangle$ versus q for the crises discussed in the text in (a) the Hénon map, $q \equiv p - p_c$, and (b) the kicked spin map, $q \equiv B - B_c$; dots — numerical results, blue solid line — theoretical fit using the theory of Sec. 3.1 with (a) $\alpha = 0.00247$, $\eta = 0.138$, $\beta = 0.107$, $a = 9.0$, $b = 3.0$, $b_E = 2.634996$, $\zeta = 1.3$, (b) $\alpha = 0.0108$, $\eta = 0.294$, $\beta = 0.125$, $a = 4.5$, $b = 2.7$, $b_E = 1.467291$, $\zeta = 3.33$.

the phase trajectory eventually enters the basin of escape (i.e. the precritical basin of attraction of the attractor at infinity) and diverges to infinity. The curve $\langle \tau(q) \rangle$, where $q \equiv p - p_c$, is shown in Fig. 1(a). It shows the basic power-law trend predicted by Eq. (1), with oscillations superimposed on it. It can be seen that the normal oscillations dominate, but weak anomalous oscillations are also present. This means that the basin of escape is almost nonfractal, and the oscillations originate mainly from the distinct fractal structure of the saddle. The normal oscillations are log-periodic with respect to $p - p_c$, which reflects the basic log-periodic fractal structure of the chaotic saddle in the collision region. The fractal structure of the basin of escape is so weak that it plays only a minor role in the occurrence of the SMR discussed further.

Another example is the kicked spin map [Hołyst & Sukiennicki, 1992a, 1992b; Kacperski & Hołyst, 1997] which describes the motion of a classical magnetic moment (spin) \mathbf{S} , $|\mathbf{S}| = S$, in the field of uniaxial anisotropy and transversal magnetic field in the form of δ -pulses with amplitude B and period $\tilde{\tau}$, $\tilde{B}(t) = B \sum_{n=1}^{\infty} \delta(t - n\tilde{\tau})$. The system is described by the Hamiltonian $H = -A(S_z)^2 - \tilde{B}(t)S_x$, where $A > 0$ is the anisotropy constant. The time evolution is determined by the Landau–Lifschitz equation with damping, $\dot{\mathbf{S}} = \mathbf{S} \times \mathbf{B}_{\text{eff}} - (\lambda/S)\mathbf{S} \times (\mathbf{S} \times \mathbf{B}_{\text{eff}})$, where $\mathbf{B}_{\text{eff}} = -dH/d\mathbf{S}$ is the effective magnetic field and $\lambda > 0$ is the damping parameter. Denoting by \mathbf{S}_n the spin vector just after the n th field pulse, the time evolution of the spin can be

written as a superposition of two-dimensional maps $\mathbf{S}_{n+1} = T_B[T_A[\mathbf{S}_n]]$, where T_A and T_B describe the motion of spin between the field pulses and the effect of the pulses, respectively. The explicit form of the maps T_A and T_B is given in Appendix A.

If B is taken as the control parameter and $S = 1$, $\tilde{\tau} = 2\pi$, $\lambda = 0.1054942\dots$, $A = 1$ are assumed, for $B < B_c = 1$ two symmetric chaotic attractors of the spin map coexist, with complementary basins of attraction, corresponding to two equivalent spin orientations, $S_z < 0$ and $S_z > 0$ (Fig. 2). At $B = B_c$ the two precritical attractors merge and a common chaotic attractor appears (Fig. 2) [Hołyst & Sukiennicki, 1992a, 1992b; Kacperski & Hołyst, 1997]. Thus in this map there are two symmetric precritical attractors and basins of attraction colliding with each other at the crisis point, and the basin of attraction of each attractor is turned into the basin of escape of the symmetric saddle. As can be seen in Fig. 2 both the precritical attractors and their basins of attraction have a distinct fractal structure. Owing to structural stability above the crisis point the fractal structures of the chaotic saddles and basins of escape will be very similar to those of the precritical attractors and their basins; in particular, the two basins of escape will be interwoven, with parts of each basins filling “holes” in the fractal structure of the symmetric basin. Above the crisis point the phase trajectory jumps chaotically between the two spin orientations, and the mean escape time $\langle \tau(q) \rangle$, where $q \equiv B - B_c$, i.e. the mean time between

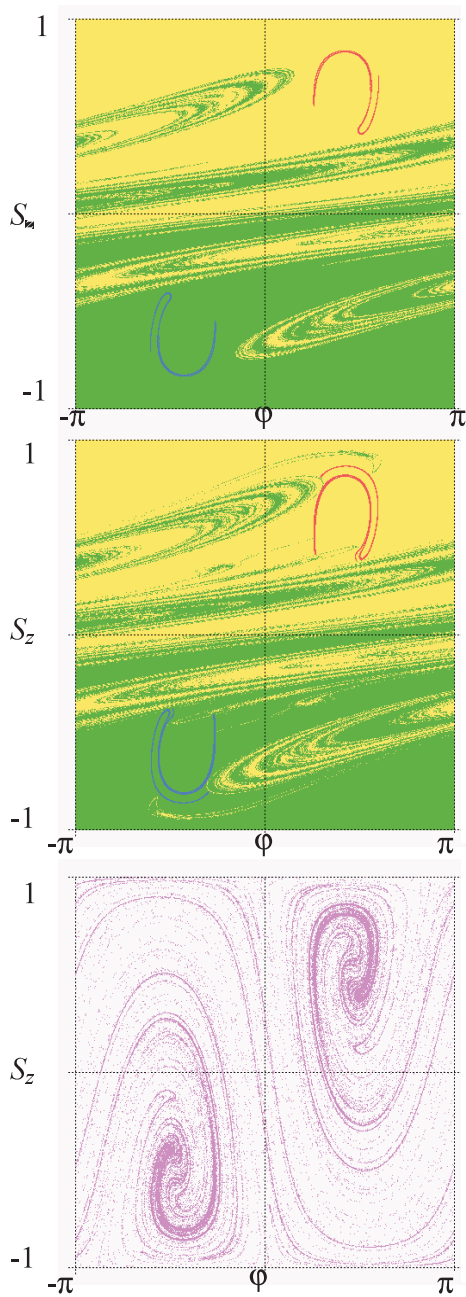


Fig. 2. The two symmetric precritical attractors and basins of attraction of the kicked spin model for $B = 0.97 < B_c$ (upper panel) and $B = 1.0 = B_c$ (middle panel); the attractor corresponding to $S_z > 0$ is red and its basin of attraction is yellow; the attractor corresponding to $S_z < 0$ is blue and its basin of attraction is green. The postcritical attractor of the kicked spin model for $B = 1.01 > B_c$ (bottom panel).

jumps, shows strong oscillations superimposed on the power-law trend [Fig. 1(b)]. In contrast with the Hénon map, here the fractal structure of the basins of escape is also distinct and the anomalous oscillations dominate. Their rough log-periodicity with

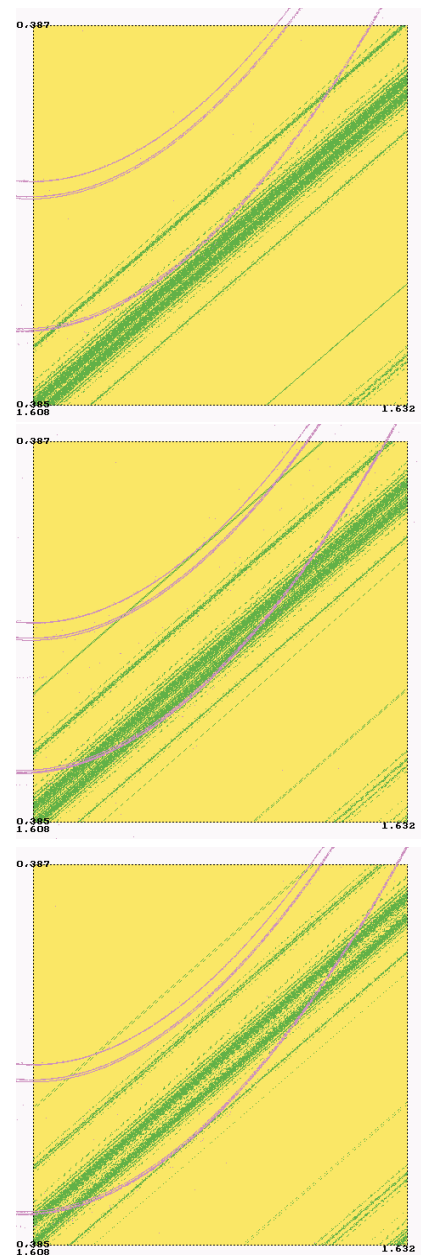


Fig. 3. Overlap of the chaotic saddle and its basin of escape above the crisis point in the kicked spin model for $B = 1.0003$ (upper panel), $B = 1.0005$ (middle panel), and $B = 1.00065$ (bottom panel); vertical axis is S_z , horizontal axis is ϕ . The chaotic saddle corresponding to the precritical attractor with $S_z > 0$ is red, its basin of escape, corresponding to the basin of attraction of the other, symmetric precritical attractor with $S_z < 0$, is green, and the complementary basin of escape of the symmetric chaotic saddle, corresponding to the basin of attraction of the precritical attractor with $S_z > 0$, is yellow (cf. Fig. 1). The branches of the chaotic saddle are shifted with the rise of the control parameter and overlap with more stripes of the basin of escape. Note that the true fractal structure of the chaotic saddles and basins of escape is more complex than in the simple models given by Eqs. (3) and (4), but the basic shape and size of the parabolic branches of the saddle and stripes of the basin is captured by the models.

respect to $B - B_c$ reflects the log-periodic fractal structure of the basins of escape in the collision region. If branches of the chaotic saddles enter parts of the fractal basins of escape, $\langle \tau \rangle$ decreases with q (Fig. 3). The sections where $\langle \tau \rangle$ rises with q appear when branches of the chaotic saddles enter “holes” in the fractal basins of escape (Fig. 3).

2.2. *Methods of analysis and numerical results*

Let us start with numerical simulations of the noise-free SR in the systems introduced in Sec. 2.1. For this purpose the control parameter q was modulated periodically, $q \rightarrow q(n) = q_0 + q_1 \cos(\omega_0 n)$, and the systems were analyzed as dynamical TC systems. The TC events were defined as the escape events, i.e. the departure of the phase trajectory towards infinity in the case of the Hénon map (after every such event the trajectory was reinjected at random on the precritical attractor and the time evolution was continued without changing the phase of the periodic signal), or jump between two equivalent spin orientations $S_z > 0$ and $S_z < 0$ in the case of the spin map. Since the periodic signal modulates the control parameter the systems studied belong to the same class as TC systems with external noise in which the information-carrying signal modulates the noise strength rather than being additive to the input [Lindner & Schimansky-Geier, 2001]. The output signal was defined as $y_n = 1$ if at time step n the TC event took place, and $y_n = 0$ otherwise. The output PSD $S(\omega)$ was evaluated from $N = 2^{15}$ points of the signal y_n . The SNR at the fundamental frequency and its higher harmonics $j\omega_0$, $j = 1, 2, 3$ was evaluated as $\text{SNR}^{(j)} = S_P(j\omega_0)/S_N(j\omega_0)$, where $S_N(j\omega_0)$ is the noise background in the vicinity of $\omega = j\omega_0$, and $S_P(j\omega_0) = S(j\omega_0) - S_N(j\omega_0)$ is the height of the peak in the PSD at $\omega = j\omega_0$.

In [Matyjaśkiewicz *et al.*, 2001; Krawiecki *et al.*, 2001] it was shown that the oscillations of the mean escape time $\langle \tau(q) \rangle$ always lead to the occurrence of noise-free SMR at the fundamental frequency, i.e. to multiple maxima of the curve $\text{SNR}^{(1)}$ versus q_0 (cf. Sec. 3.2). The location and height of the maxima of the $\text{SNR}^{(1)}$ can be directly related to the shape of the functional dependence of $\langle \tau \rangle$ on q . In turn, in this paper we aim at extension of the latter results by establishing connections between the curves SNR versus q_0 at subsequent harmonics.

Exemplary curves $\text{SNR}^{(j)}$, $j = 1, 2, 3$, versus the control parameter for the Hénon and the spin map are shown in Fig. 4. In Figs. 4(a) and 4(d) noise-free SMR at the fundamental frequency is clearly seen. In order to extend the investigation of the SMR to higher harmonics, let us first observe that for $j = 2, 3$ dips appear, i.e. points where $\text{SNR}^{(j)} = 0$, and that the total number of maxima of the SNR increases when going from the lower to higher harmonics. From the numerical results in Fig. 4 the following correspondence rules between the maxima and dips of the SNR at subsequent harmonics can be deduced. First, the dips of the $\text{SNR}^{(j+1)}$ appear roughly at the same locations as the broad, smooth maxima of the $\text{SNR}^{(j)}$; such dips separate two neighboring maxima of the $\text{SNR}^{(j+1)}$. This can be easily seen in the case of the Hénon map: cf. the location of the maxima and dips labeled by b, c, d, e in Figs. 4(a)–4(c). Second, narrow sharp peaks of the $\text{SNR}^{(j+1)}$ can appear at the same location as sharp peaks of the $\text{SNR}^{(j)}$. This can be seen in the case of the spin map: cf. the location of peaks labeled by f, g in Figs. 4(d)–4(f). Justification of these rules will be given in Sec. 4.1. At this point let us only mention that the first above-mentioned rule resembles the analogous correspondence between the maxima and dips of the SNR at subsequent harmonics in TC stochastic resonators with external noise [Loerincz *et al.*, 1999]. In such systems (with only one maximum of the $\text{SNR}^{(1)}$) dips of the $\text{SNR}^{(j+1)}$ appear at similar noise intensities as smooth maxima of the $\text{SNR}^{(j)}$. The basic difference with the case of noise-free SMR is that in the latter case the control parameter is varied instead of the external noise intensity, and that there are multiple maxima of the SNR at the fundamental frequency which results in multiple dips of the SNR already at the first harmonic.

3. Theory for the Signal-to-Noise Ratio at Higher Harmonics

3.1. *Theory for the model systems with crises*

Before discussing the above-mentioned numerical results in more detail, in this section we derive analytic formulae for the SNR at the fundamental frequency and its higher harmonics versus q_0 for a class of systems introduced in Sec. 2. The following theory is an extension of the theory for the SNR at the fundamental frequency [Matyjaśkiewicz *et al.*,

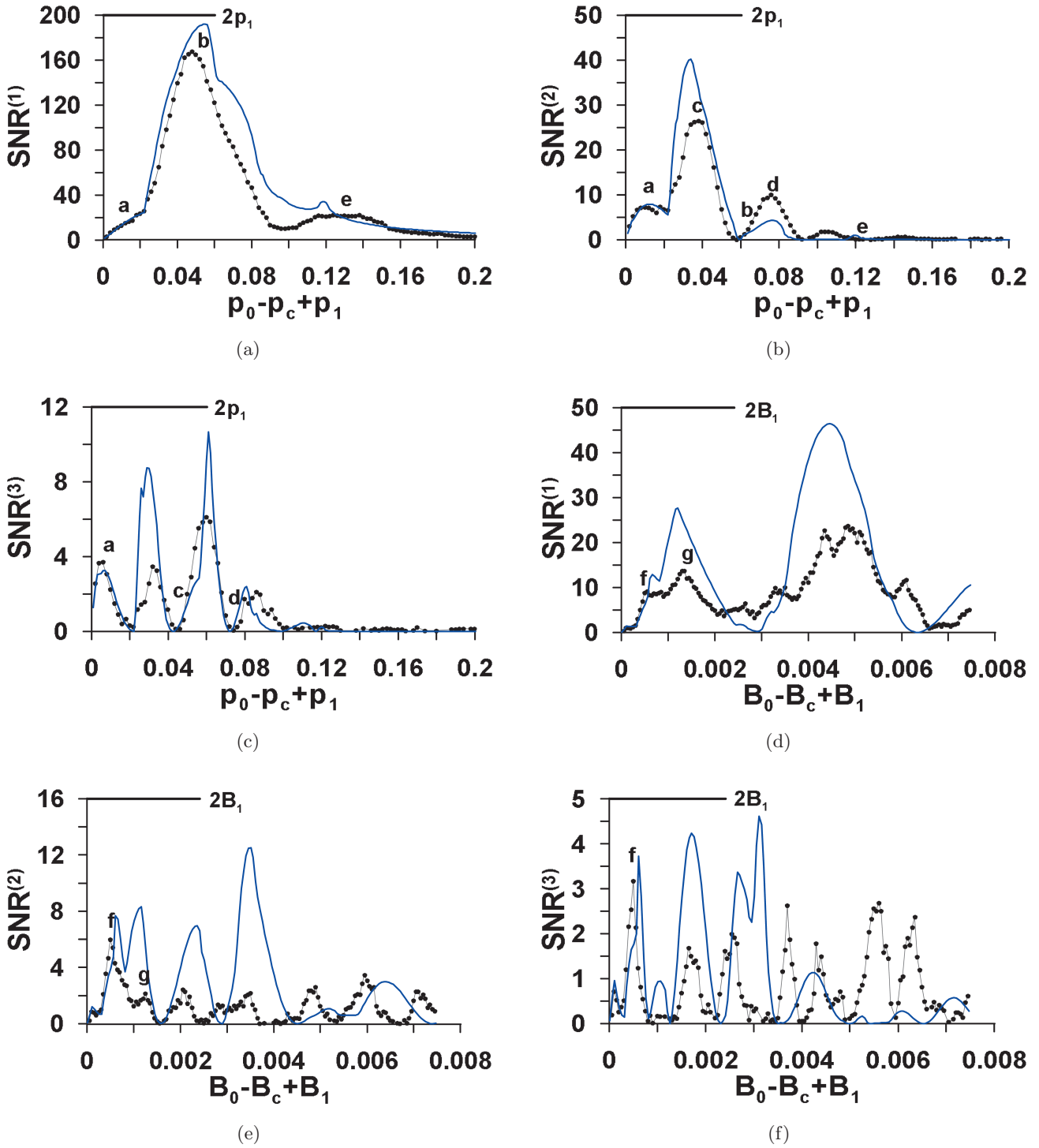


Fig. 4. $\text{SNR}^{(j)}$, $j = 1, 2, 3$, versus $q_0 + q_1$ for (a)–(c) the Hénon map with $p_1 = 0.03$, and (d)–(f) the spin map with $B_1 = 1.2 \times 10^{-3}$; dots — numerical results, blue solid line — theoretical fit using the theory of Sec. 3.1 with the parameters as in Fig. 1. The objects labeled with the same letters correspond to each other as discussed in Sec. 4.3, the bars have length $2q_1$.

2001] valid under the same assumptions (the system is close to crisis and the amplitude q_1 is small) and based on the same simple models of the fractal chaotic saddle and the basin of escape.

In the adiabatic approximation $\omega_0 \rightarrow 0$ the SNR at the j th harmonic $\text{SNR}^{(j)}$ can be obtained from the time-dependent TC probability $p(n) = \Pr(y_n = 1) \equiv p(q_0 + q_1 \cos(\omega_0 n))$ using the formula

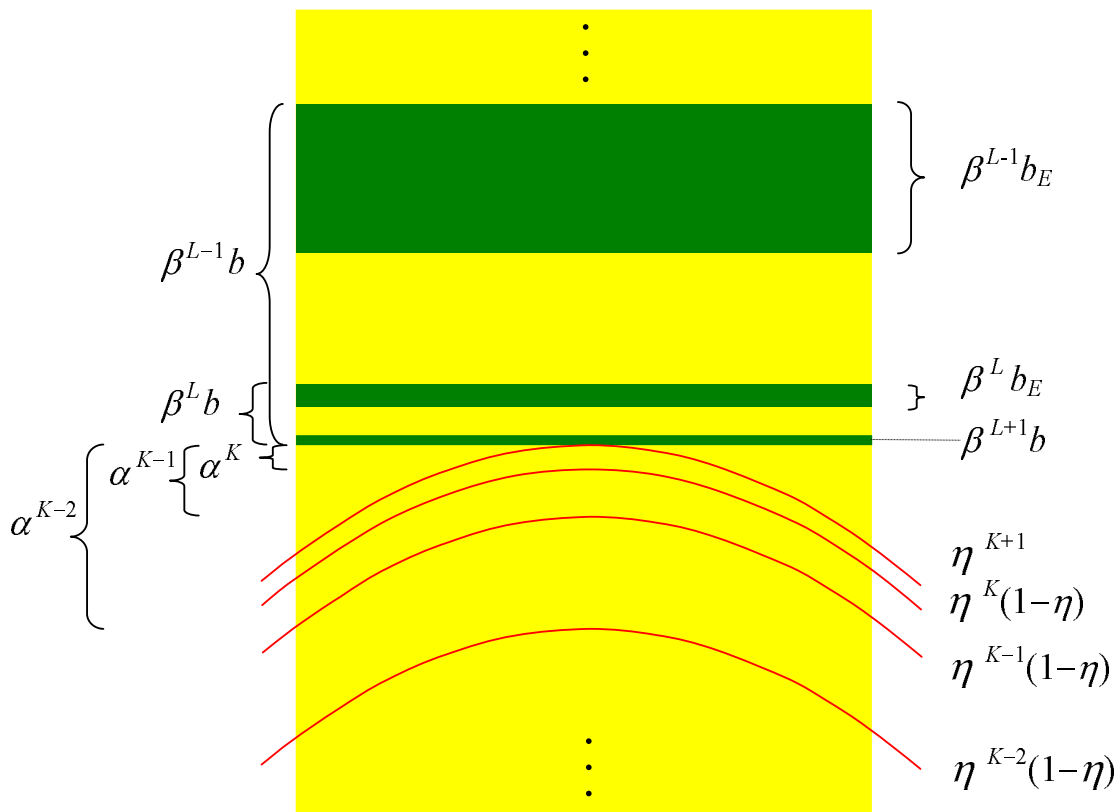


Fig. 5. The model of the fractal chaotic saddle and the fractal basin of escape as defined in Eqs. (3) and (4); the colors correspond to those in Fig. 3.

[Chapeau-Blondeau, 1995; Chapeau-Blondeau & Godivier, 1997]

$$\text{SNR}^{(j)} = MT_0 |P_j|^2 / (\bar{p} - \bar{p}^2) \approx MT_0 |P_j|^2 / \bar{p}, \quad (2)$$

where $P_j = T_0^{-1} \sum_{n=0}^{T_0-1} p(n) \exp(-ij\omega_0 n)$ is the j th Fourier coefficient of $p(n)$, $T_0 = 2\pi/\omega_0$ is the period of the external signal, M is the number of periods within the time interval from which the data were stored (in our numerical simulations, $M = N/T_0 = 2^{15}/T_0$), and the bar denotes the time average over T_0 . The approximate equality holds for $p(n) \ll 1$ which is true in systems close to crisis. In Eq. (2) the SNR is evaluated taking into account the finite frequency resolution of the PSD $\Delta f = 1/MT_0$ [McNamara & Wiesenfeld, 1989] so it can be directly compared with the SNR obtained numerically.

In systems with crises in the first approximation, neglecting the oscillations, the TC probability

can be assumed as $p(n) = 1/\langle \tau(q_0 + q_1 \cos \omega_0 n) \rangle$, where $\langle \tau(q) \rangle$ is given by Eq. (1). In order to take into account the oscillations of the TC probability we introduce a model approximating the fractal structures of the chaotic saddle and the basin of escape in the collision region above the crisis point $q = q_c$ [Kacperski & Holyst, 1999a, 1999b] (Fig. 5); without loss of generality we assume $q_c = 0$. The assumption of our model is that the topological and metric properties of these sets above the crisis point are identical with those of the corresponding precritical sets: the precritical attractor and the basin of attraction, respectively. The effect of the increase of the control parameter is only the shift of the relative position of the chaotic saddle and the basin of escape. Let us start with the case when the control parameter q is constant in time. The suitable model of the chaotic saddle \mathcal{A} is a family of $K + 2$ parabolic segments \mathcal{A}_k

$$\mathcal{A} = \bigcup_{k=0}^{K+1} \mathcal{A}_k = \bigcup_{k=0}^{K+1} \{(x, y) : y = -x^2 - (1 - \delta_{k, K+1}) a \alpha^k + q\}, \quad (3)$$

with the relative density of invariant measure $\tilde{\mu}_k = (1 - \eta)\eta^k$ for $0 \leq k \leq K$ and $\tilde{\mu}_{K+1} = \eta^{K+1}$, where $a > 0$ and $\alpha, \eta \in (0, 1)$ are model parameters. The model (3) reproduces well the shape of the branches of the chaotic saddle in the collision

$$\mathcal{B} = \bigcup_{l=0}^{L+1} \mathcal{B}_k = \bigcup_{l=0}^{L+1} \{(x, y) : (1 - \delta_{l,L+1})(\beta^l b - \beta^l b_E) \leq y \leq \beta^l b\}, \quad (4)$$

where $b > 0$, $0 < b_E < b$ and $\beta \in (0, 1)$ are again model parameters. Again, the model (4) approximates well the shape of the stripes of the basin of escape in the collision region (cf. Fig. 3) and their basic log-periodic structure, with period $\log \beta$, reflected in Fig. 1(b). Taking larger K, L means to take a finer approximation of the infinite fractal sets. The parabolic segments as well as stripes accumulate at the line $y = 0$ at the crisis threshold $q = q_c = 0$. As q increases, the chaotic saddle overlaps the basin of escape. The TC probability is proportional to the measure of the overlap, i.e. the total length of the parabolic segments inside all stripes times their relative measure densities, $p(q) = \zeta \mu(q)$, $\zeta = \text{const}$. The function $\langle \tau(q) \rangle = 1/p(q)$ obtained in such a way shows the power law trend with the scaling exponent $\gamma = \log \eta / \log \alpha + 1/2$ [Kacperski & Holyst, 1999a, 1999b], and with irregular oscillations superimposed on it. The model parameters α, β, η can be evaluated from the eigenvalues of the periodic orbit mediating in the crisis or measured from the magnified plots of the collision region between the chaotic saddle and the basin of escape, like those in Fig. 3. The model curves can be then fitted to the numerical data by choosing properly the parameters a, b and ζ (Fig. 1). For the case of periodically modulated control parameter the replacement $q \rightarrow q_0 + q_1 \cos(\omega_0 n)$ is made in Eq. (3) and the time-dependent escape probability is obtained as

$$p(n) = \zeta \mu(q_0 + q_1 \cos(\omega_0 n)) = \zeta \sum_{k=0}^{K+1} \sum_{l=0}^{L+1} \mu_{kl}(n), \quad (5)$$

where the last term is a sum of contributions to the TC probability from the segments \mathcal{A}_k overlapping the stripes \mathcal{B}_l . Performing the time averaging and Fourier transforming the above equation one obtains that \bar{p} and P_j are similar sums

region (cf. Fig. 3) and takes into account the basic log-periodic, with period $\log \alpha$, structure of the saddle which can be deduced from the mean escape times in Fig. 1. The model of the basin of escape \mathcal{B} is a family of $L + 2$ stripes \mathcal{B}_l

of contributions

$$\bar{p} = \zeta \sum_{k=0}^{K+1} \sum_{l=0}^{L+1} \bar{\mu}_{kl}, \quad P_j = \zeta \sum_{k=0}^{K+1} \sum_{l=0}^{L+1} M_{kl,j}. \quad (6)$$

The contributions $\bar{\mu}_{kl}$ and $M_{kl,j}$ can be evaluated analytically in the adiabatic approximation in the limit of small $q_0 + q_1$; the results are given in Appendix B.

3.2. General remarks and simple approximations for the SNR

The theory of Sec. 3.1 is exact, however, limited only to the case of the model for fractal-induced oscillations of the mean TC probability. Besides, the expressions in Eq. (6) are complex and do not allow simple analysis of the curves $\text{SNR}^{(j)}$ versus q_0 . In this section approximate treatment of the problem of SMR in a certain class of TC systems is presented, based on direct examination of the dependence of the TC probability on a control parameter q [Krawiecki *et al.*, 2001], which explains the origin of SMR in this class of systems.

We consider TC systems in which the TC probability depends on a parameter q , to which a small, slowly varying periodic signal is then added, so that the time-dependent TC probability is $p(n) = p(q_0 + q_1 \cos(\omega_0 n))$. In order to evaluate $\text{SNR}^{(j)}$ one has to obtain the Fourier coefficients P_j of $p(n)$, which in the continuous-time approximation are functionals of $p(q)$ on the interval $(q_0 - q_1, q_0 + q_1)$. If $p(q)$ is an analytic function on this interval, $p(n)$ can be expanded in the Taylor series around q_0 with respect to $q_1 \cos(\omega_0 n)$ which yields

$$p(n) = p(q_0) + q_1 \left. \frac{dp}{dq} \right|_{q_0} \cos(\omega_0 n) + \frac{1}{2} q_1^2 \left. \frac{d^2 p}{dq^2} \right|_{q_0} \cos^2(\omega_0 n) \quad (7)$$

$$+ \frac{1}{6} q_1^3 \left. \frac{d^3 p}{dq^3} \right|_{q_0} \cos^3(\omega_0 n) + \dots$$

However, Eq. (7) does not approximate well the function $p(n)$ for a given q_0 if $p(q)$ varies fast, or is not differentiable on the interval $(q_0 - q_1, q_0 + q_1)$; it can be so, e.g. in the case of the curves in Fig. 1. Then it is better to replace the derivatives in Eq. (7) with a sort of “average” derivatives on this interval. They, in turn, can be approximated as difference quotients, so that Eq. (7) takes a form

$$\begin{aligned} p(n) &\approx p(q_0) + q_1 p^{(1)}|_{q_0} \cos(\omega_0 n) \\ &+ \frac{1}{2} q_1^2 p^{(2)}|_{q_0} \cos^2(\omega_0 n) \\ &+ \frac{1}{6} q_1^3 p^{(3)}|_{q_0} \cos^3(\omega_0 n) + \dots \end{aligned} \quad (8)$$

where $p^{(1)}|_{q_0} = [p(q_0 + q_1) - p(q_0 - q_1)]/(2q_1)$, $p^{(2)}|_{q_0} = [p(q_0 + q_1) - 2p(q_0) + p(q_0 - q_1)]/(2q_1)^2$, etc., are difference quotients of the first, second, etc., order evaluated at the interval $(q_0 - q_1, q_0 + q_1)$. Evaluating the Fourier components of $p(n)$ from the above expansions it can be seen that in the first approximation P_j at q_0 is proportional to $(d^j p/dq^j)|_{q_0}$, or, in a general case, to the respective difference quotient $p^{(j)}|_{q_0}$. Neglecting the dependence on \bar{p} , the $\text{SNR}^{(j)}$ given by Eq. (2) is proportional to $|P_j|^2$.

The above expansions, together with Eq. (2), prove that if the TC probability has the “average” derivative of order j which is a nonmonotonic function of the control parameter q , multiple maxima of the SNR at the j th harmonic will occur. Hence, if $p^{(1)}$ is a nonmonotonic function of q , SMR at the fundamental frequency will appear. In particular, distinct, broad maxima of the SNR at the fundamental frequency can be associated with oscillations of $p(q)$ wider than $2q_1$ around a general rising trend, since then $p^{(1)}|_{q_0}$ has certainly an extremum at some q_0 in the range of the oscillation. Narrow oscillations of $p(q)$ result only in small peaks or modulation of the slope of the SNR. The above condition defines a whole class of TC systems in which SMR occurs in the adiabatic limit of slowly varying signals. From Fig. 1 it is clear that the chaotic maps close to crisis, with fractal-induced oscillations of the mean escape time, belong to this class. Since the width of the oscillations in the latter systems increases on average logarithmically with $q - q_c$, broad oscillations of $\langle \tau(q) \rangle$, and thus distinct maxima of the $\text{SNR}^{(1)}$, can appear, approximately, only for $q_0 \geq 2q_1$, far

enough from the crisis threshold, which is roughly confirmed by Figs. 4(a) and 4(d).

The proportionality of the $\text{SNR}^{(j)}$ to the difference quotient $p^{(j)}$ also explains why there are more maxima of the SNR at higher harmonics. For example, by definition, $p^{(1)}|_{q_0}$ depends only on the values of $p(q)$ at $q = q_0 \pm q_1$, while $p^{(2)}|_{q_0}$ depends also on $p(q_0)$. In general, $p^{(j)}|_{q_0}$ depends on the value of $p(q)$ in j points on the interval $(q_0 - q_1, q_0 + q_1)$. This amounts to more sensitive probing of the function $p(q)$ on this interval, which reveals even narrow oscillations of the TC probability as clear maxima of the SNR at higher harmonics.

4. Discussion

4.1. Relationships between the SNR at consecutive harmonics

Taking advantage of the expansions in Eq. (7) and (8), certain relationships between the SNR at subsequent harmonics in TC systems can be also deduced. In the discussion below, derivatives should be understood in the sense of “average” derivatives approximated by the difference quotients in the case of nonanalytic or fast varying functions $p(q)$. If at some q_0 the curve P_j has a distinct, broad extremum characterized by $dP_j/dq|_{q_0} \approx (d^{j+1}p/dq^{j+1})|_{q_0} = 0$, at the same q_0 there should be $P_{j+1} = 0$. This condition defines the location of dips of the curve $\text{SNR}^{(j+1)}$ versus q_0 , defined as points where $\text{SNR}^{(j+1)} = 0$. Since the $\text{SNR}^{(j)}$ is proportional to $|P_j|^2$ [Eq. (2)], the extrema of P_j correspond to maxima of the $\text{SNR}^{(j)}$. Hence, the dips of the $\text{SNR}^{(j+1)}$ should appear approximately for such q_0 that the curve $\text{SNR}^{(j)}$ has distinct maxima. Similarly, if at a certain q_0 the derivative $(dP_j/dq)|_{q_0} \approx (d^{j+1}p/dq^{j+1})|_{q_0}$ has an extremum, at the same q_0 an extremum of the curve P_{j+1} versus q_0 appears. This condition defines the location of the maxima of the $\text{SNR}^{(j+1)}$: they should be associated with inflexion points of the curve $\text{SNR}^{(j)}$ versus q_0 . When applied to the model systems from Sec. 2, the above arguments explain the correspondence between the broad maxima and dips of the SNR at subsequent harmonics in Fig. 4, noticed in Sec. 2.2. As mentioned above, such distinct maxima of the SNR, as well as clear inflexion points, appear only for large enough q_0 , far from the crisis threshold, and the correspondence rule is true in this region. On the other hand, if at some q_0 the function P_j has a narrow extremum, whose width is smaller than $2q_1$, so that

the $\text{SNR}^{(j)}$ has a narrow peak, the difference quotient $p^{(j+1)}$ (mimicking the local derivative of P_j , but on the interval wider than the peak width) need not be zero at this q_0 . This means that the $\text{SNR}^{(j+1)}$ need not have dips at the locations of narrow maxima of the $\text{SNR}^{(j)}$. In contrast, it can happen that $p^{(j+1)}$ has a narrow extremum close to this point, too. Then both curves $\text{SNR}^{(j)}$ and $\text{SNR}^{(j+1)}$ have maxima at the same point. This explains the correspondence between the narrow, sharp peaks of the SNR at consecutive harmonics found in the model systems in Sec. 2.2. As mentioned above, narrow peaks of, e.g. the SNR at the fundamental frequency can be connected with narrow oscillations of $p(q)$. Such a situation is impossible in generic TC systems with noise [Loerincz *et al.*, 1999], in which the TC probability is always a smooth, slowly varying function of the noise intensity.

4.2. Influence of the fractal structures on the SNR at the fundamental frequency and higher harmonics in the model systems

In this section we constrain our attention to the model case of chaotic maps with fractal precritical attractors and basins of attraction, colliding at the crisis point. On the basis of the analytic theory of Sec. 3.1 and general considerations of Secs. 3.2 and 4.1, we analyze the origin of simple “building blocks” (maxima and dips) of the SNR versus q_0 curves at subsequent harmonics of the fundamental frequency. This aims at providing intuition on how the overlap of the parabolic segments of the chaotic saddle and stripes of the basin of escape leads to complex curves in Fig. 4.

Let us start with a simple case and neglect the fractal structure of the chaotic saddle and basin of escape at crisis. The mean TC time is then given by Eq. (1). As a simple example let us take a single parabolic segment \mathcal{A}_0 entering the half-plane $y > 0$ which yields $\gamma = 0.5$ in Eq. (1); the results are similar for $\gamma > 0.5$ which is always fulfilled for two-dimensional maps [Grebogi *et al.*, 1986; Grebogi *et al.*, 1987]. In Fig. 6 the curves $\text{SNR}^{(j)}$, $j = 1, 2, 3$, obtained using the theory of Sec. 3.1 are shown. By inspection of the difference quotient $p^{(1)}$ it can be easily proved that $|P_1|$ has a single maximum at $q_0 \approx q_1$ [Krawiecki *et al.*, 2001]. The maximum of the $\text{SNR}^{(1)}$ in

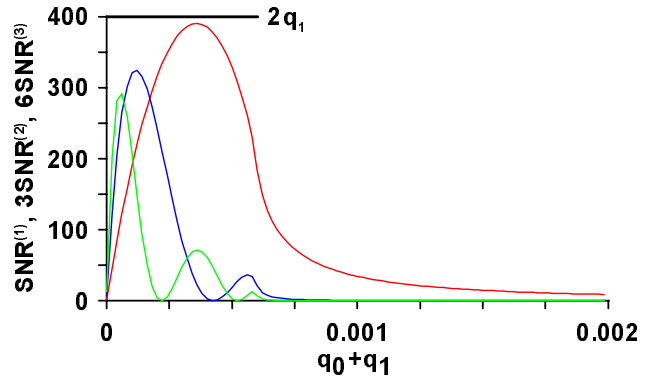


Fig. 6. $\text{SNR}^{(j)}$, $j = 1, 2, 3$ versus $q_0 + q_1$ for a single parabolic segment \mathcal{A}_0 entering the half-plane $y > 0$, and for $q_1 = 3 \times 10^{-4}$, $\zeta = 3.3$; red line — $\text{SNR}^{(1)}$, blue line — $3 \times \text{SNR}^{(2)}$, green line — $6 \times \text{SNR}^{(3)}$.

Fig. 6 corresponds to this maximum of $|P_1|$. The correspondence between the distinct maxima and dips, and between the inflexion points and maxima of the $\text{SNR}^{(j)}$ at subsequent harmonics, predicted in Sec. 4.1, is only approximate. This is mainly because the maxima of the $\text{SNR}^{(j)}$ do not appear exactly for q_0 such that P_j has analytic extrema, due to the dependence of the $\text{SNR}^{(j)}$ on \bar{p} [Eq. (2)] which is a function of q_0 , too. Besides, for higher j the contributions to P_j from the terms of order $j' > j$ in Eqs. (7) and (8) become significant, which have not been taken into account in the discussion in Sec. 4.1.

For the nonfractal chaotic saddle and basin of escape the curves $\text{SNR}^{(j)}$ versus q_0 are relatively simple and very similar to those observed in TC systems versus external noise intensity [Loerincz *et al.*, 1999]. In particular, there is only one smooth maximum of the $\text{SNR}^{(1)}$ versus q_0 . Let us now consider how the presence of the fractal structures complicates the shape of the SNR at the fundamental frequency and higher harmonics. This will be done separately for the case of the fractal attractor and the fractal basin of escape.

To analyze the effect of the fractal structure of the saddle we take $K+1 = 1$ in Eq. (3) and consider two parabolic segments $\mathcal{A}_0, \mathcal{A}_1$, distant by a , entering the half-plane $y > 0$ modeling the nonfractal basin of escape. For simplicity, only the SNR versus q_0 at the fundamental frequency and its first harmonic for this case are shown in Fig. 7 for decreasing a . If $a \geq 2q_1$ there are two separate distinct, smooth maxima of the $\text{SNR}^{(1)}$, located at $q_0 \approx q_1$ and $q_0 \approx q_1 + a$ [Krawiecki *et al.*, 2001], connected with \mathcal{A}_1 and \mathcal{A}_0 , respectively. To each of these maxima the correspondence rules from Sec. 4.1 between the

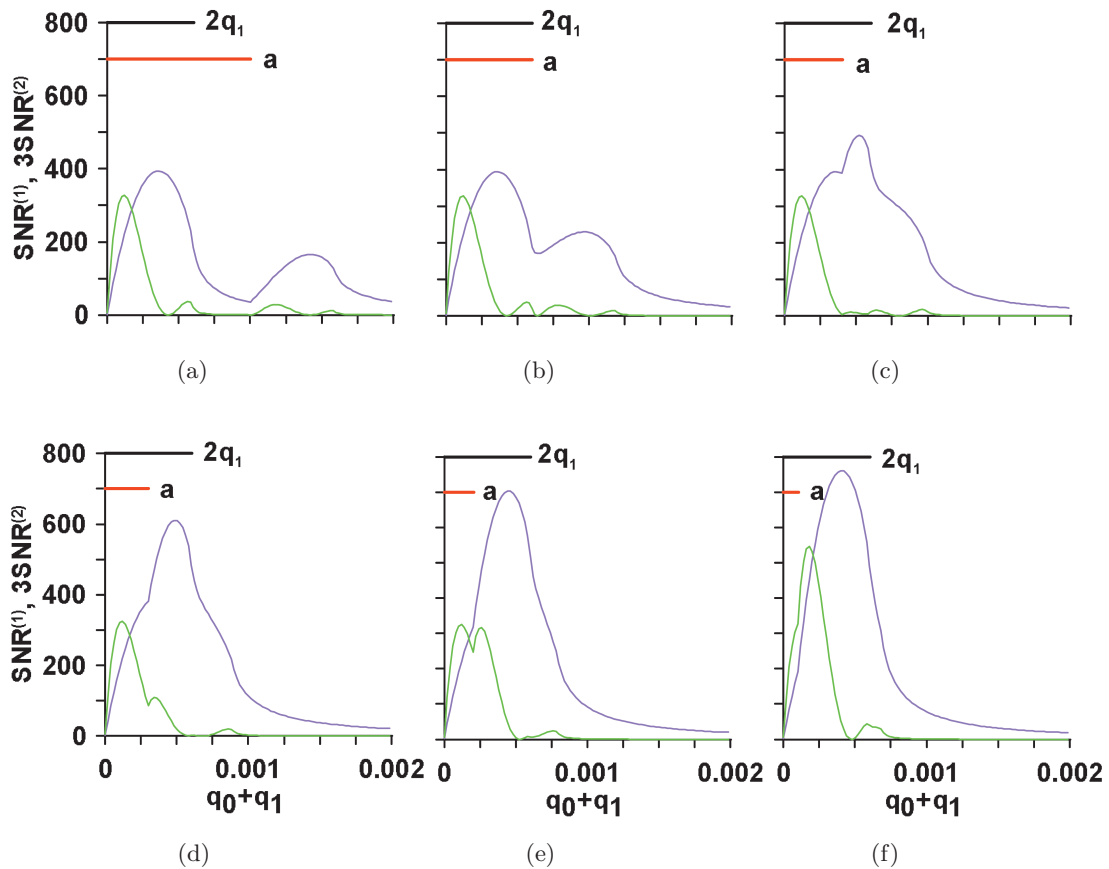


Fig. 7. $\text{SNR}^{(j)}$, $j = 1, 2$ versus $q_0 + q_1$ for two parabolic segments \mathcal{A}_0 , \mathcal{A}_1 , distant by a , entering the half-plane $y > 0$, and for $q_1 = 3 \times 10^{-4}$, $\eta = 0.5$, $\zeta = 3.3$, (a) $a = 10^{-3}$, (b) $a = 6 \times 10^{-4}$, (c) $a = 4 \times 10^{-4}$, (d) $a = 3 \times 10^{-4}$, (e) $a = 2 \times 10^{-4}$, (f) $a = 10^{-4}$; violet line — $\text{SNR}^{(1)}$, green line — $3 \times \text{SNR}^{(2)}$, the bars have lengths $2q_1$ (black) and a (red).

distinct maxima and dips, and the inflexion points and maxima of the SNR at subsequent harmonics can be applied separately. Hence there are two dips of the $\text{SNR}^{(2)}$ located at similar q_0 as the maxima of the $\text{SNR}^{(1)}$, and four maxima of the $\text{SNR}^{(2)}$, the three most rightward corresponding to the inflexion points of the $\text{SNR}^{(1)}$ [Figs. 7(a) and 7(b)]. As a is decreased below $2q_1$ the maxima in both curves merge [Figs. 7(c)–7(f)]. The number of distinct maxima decreases; instead, the slopes of the remaining maxima are slightly modulated. Since the maxima of the $\text{SNR}^{(2)}$ are narrower, the neighboring maxima can remain distinct and smooth even for $a \ll 2q_1$, although the maxima of the $\text{SNR}^{(1)}$ had already merged [Figs. 7(d) and 7(e)].

The effect of the fractal structure of the basin of escape can be analyzed using a model Eq. (3) with $K + 1 = 0$ and Eq. (4) with $L + 1 = 0$, i.e. one parabolic segment \mathcal{A}_0 entering a single stripe \mathcal{B}_0 located at $0 < y < b$. The SNR versus q_0 at the fundamental frequency and its first harmonic are

shown in Fig. 8 for decreasing b . If $b \geq 2q_1$ there are two distinct, smooth maxima of the $\text{SNR}^{(1)}$: one located at $q_0 \approx q_1$ and connected with the oscillations of the top of the parabolic segment (under the influence of the periodic forcing) within the stripe, and another at $q_0 \approx q_1 + b$, connected with the oscillations of this top above the stripe [Krawiecki *et al.*, 2001]. The correspondence rules of Sec. 4.1 apply to each maximum separately so that there are two dips and four maxima of the $\text{SNR}^{(2)}$ located as expected [Figs. 8(a) and 8(b)]. As b is decreased approximately below $2q_1$, the first maximum of the $\text{SNR}^{(1)}$ is cut and turns into a sharp nonanalytic peak at $q_0 = b - q_1$ [Figs. 8(c)–8(f)]. This is because the stripe is too narrow and the top of the parabolic segment cannot for any q_0 remain within the stripe during the whole period of the periodic forcing. Similarly, the first maximum of the $\text{SNR}^{(2)}$ is also cut and turned into a sharp peak, but for smaller b [Fig. 8(f)]. In the latter case the sharp peaks of both curves appear at the same $q_0 = b - q_1$,

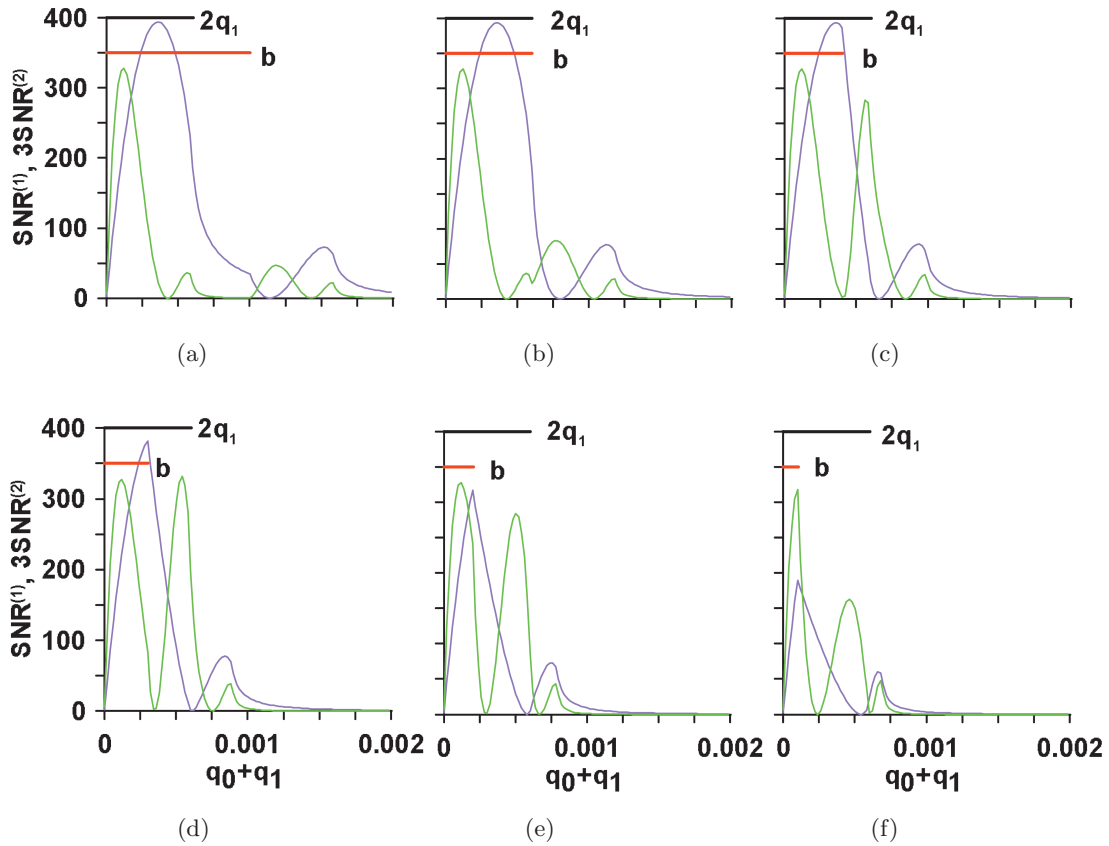


Fig. 8. $\text{SNR}^{(j)}$, $j = 1, 2$ versus $q_0 + q_1$ for a parabolic segment \mathcal{A}_0 entering the stripe \mathcal{B}_0 located at $0 < y < b$, and for $q_1 = 3 \times 10^{-4}$, $\zeta = 3.3$, (a) $b = 10^{-3}$, (b) $b = 6 \times 10^{-4}$, (c) $b = 4 \times 10^{-4}$, (d) $b = 3 \times 10^{-4}$, (e) $b = 2 \times 10^{-4}$, (f) $b = 10^{-4}$; violet line — $\text{SNR}^{(1)}$, green line — $3 \times \text{SNR}^{(2)}$, the bars have lengths $2q_1$ (black) and b (red).

and the dip of the $\text{SNR}^{(2)}$ is located further to the right rather than at the location of the first peak of the $\text{SNR}^{(1)}$.

From Figs. 7 and 8 it can be seen that the collision of fractal structures at crisis leads to multiple maxima of the SNR at all harmonics. The collision of fractal structures whose scale (the largest relevant distance) is larger than, approximately, $2q_1$ (both wide stripes and distant parabolic segments) results in broad, smooth maxima of the SNR at the fundamental frequency and its lower harmonics. The multiple broad, smooth maxima of the $\text{SNR}^{(j)}$ correspond in general to multiple dips of the $\text{SNR}^{(j+1)}$. The fractal structure of the chaotic saddle at a scale smaller than $2q_1$ leads mainly to the modulation of the slope of the SNR curves, or to the appearance of narrow and smooth maxima of the SNR both at the fundamental frequency and its higher harmonics. The fractal structure of the basin of escape at a scale smaller than $2q_1$ can in turn lead to the appearance of sharp nonanalytic peaks of the SNR. Such peaks can appear at the

same values of the control parameter at consecutive harmonics. In general the curves $\text{SNR}^{(j)}$ result from the superposition of many basic events like in examples above occurring simultaneously on different scales. This leads to complex structures of the SNR versus q_0 like in Fig. 4.

4.3. Discussion of numerical results and comparison with theory

The origin of certain maxima and dips of the numerical curves of the SNR at higher harmonics in Fig. 4 can be traced using the simplified examples of Sec. 4.2. The objects corresponding to each other in Fig. 4 are labeled by identical letters.

The case of the Hénon map is simpler to analyze since the basin of escape is almost nonfractal and only smooth maxima connected with subsequent branches of the fractal chaotic saddle entering the basin of escape are visible in the curves $\text{SNR}^{(j)}$, $j = 1, 2, 3$. The effect of the weak structure of

the basin of escape can be neglected in this case. The maxima b and e of the $\text{SNR}^{(1)}$ in Fig. 4(a) are broad and resemble those in Fig. 7(a). To each of these maxima correspond dips b and e of the $\text{SNR}^{(2)}$ in Fig. 4(b), each separating two maxima. A similar correspondence between the maxima c and d in Fig. 4(b) and dips of the $\text{SNR}^{(3)}$ in Fig. 4(c) can be seen. Besides, the object a in Fig. 4(a) is a remainder of a maximum which merged with the maximum b , but there are still narrower maxima of the SNR at higher harmonics in Figs. 4(b) and 4(c), like in Figs. 7(d) and 7(e).

In the case of the spin map many sharp peaks in the curves $\text{SNR}^{(j)}$, $j = 1, 2, 3$ can be seen. For example, these are peaks f and g of the curve $\text{SNR}^{(1)}$ in Fig. 4(d) and corresponding peaks of the SNR at the second and, possibly, third harmonic in Figs. 4(e) and 4(f). These peaks appear in the SNR at all harmonics for the same B_0 which resembles the relative location of maxima in Fig. 8(f). The origin of peaks and maxima of the SNR for higher values of B_0 are difficult to explain using simple examples of Sec. 4.2. This is because the amplitude B_1 is high and every peak and maximum are a result of overlap of many branches and stripes belonging to two complex incommensurate fractal structures. However, the amplitude of the periodic signal has to be high enough in order to obtain reliable numerical results for the SNR at higher harmonics which are much lower than the SNR at the fundamental frequency.

The agreement between numerical and theoretical results based on the theory of Sec. 3.1 is quantitatively good for the Hénon map [Figs. 4(a)–4(c)] and qualitatively good for the spin map [Figs. 4(d)–4(f)]. The latter discrepancy is again a result of the high value of B_1 , and the fact that the models of Sec. 3.1 neglect further fine branching of the parabolic segments and stripes in real fractal chaotic saddles and basins of escape (Fig. 3) [Matyjaśkiewicz *et al.*, 2001].

5. Fractal Spectroscopy

The oscillations of the mean escape time and multiple maxima of the SNR in noise-free SMR in the investigated maps close to crisis are deeply rooted in the fractal structures of the precritical attractors and, possibly, basins of attraction in the collision region. Oscillations of $\langle \tau \rangle$ and maxima of the SNR of different shape and width correspond to the collision of fractal structures of different origin and

scale. Thus, by direct thorough inspection of such curves, it is possible to reconstruct, e.g. the local (in the collision region) distribution of invariant measure on the precritical attractor, or the local mean log-periodicity of the fractal branches and stripes of the chaotic saddle or basin of escape. Using this information, one can deduce the important parameters of the model equations (3) and (4) from the measurement of $\langle \tau \rangle$ or the SNR, without the need to examine directly the collision region or the eigenvalues of the periodic orbit mediating in crisis. While for the two-dimensional maps the gain in the time of numerical simulations need not be significant, there are experimental systems close to crisis in which the oscillations of the mean escape time are probably fractal-induced [Sommerer & Grebogi, 1992]. In fact, at least normal oscillations should be quite common, since the precritical attractors are always fractal sets. In the experiment it is usually difficult to investigate the local structure of colliding sets directly, but it can be examined indirectly, from the measurements of experimentally available quantities which can be obtained by simple changes of the control parameter. We call these methods of indirect measurements “fractal spectroscopy”.

In fact, the whole information about the two colliding sets is contained in the curves $\langle \tau(q) \rangle$. From the width of normal and anomalous oscillations the parameters α , β in Eqs. (3) and (4) can be obtained, and the parameter η can be evaluated from the slope of the curve $\langle \tau(q) \rangle$ and the relationship $\gamma = \log \eta / \log \alpha + 1/2$ [Kacperski & Hołyst, 1999b]. Since $\text{SNR}^{(1)} \propto |(dp/dq)|_{q_0}|^2$ even small oscillations of the mean escape time lead to large changes of the SNR, and the effect of fractal structures on SMR is easily visible and more spectacular. However, only oscillations of $\langle \tau \rangle$ far from the crisis threshold, whose width is larger than $2q_1$, lead to distinct maxima of the SNR. Location of these maxima shows also log-periodicity connected with the dominating oscillations of the mean escape time (shifted only approximately by q_1 with respect to that of $\langle \tau(q) \rangle$, cf. Figs. 7(a) and 8(a)), although in the case of dominating anomalous oscillations it may be difficult to distinguish between the maxima related to entering and leaving the stripes of the basin of escape by the segments of the chaotic saddle [Fig. 8(a)]. Thus the parameters α and β in Eqs. (3) and (4) can be in principle obtained from the data on SR. On the other hand, collision of tiny fractal structures whose scale is smaller than $2q_1$ leads to narrow oscillations

of $\langle\tau(q)\rangle$ located mainly close to the crisis threshold, and to the modulation of the slope or narrow peaks of the SNR⁽¹⁾ which are difficult to interpret. The amplitude q_1 , although small, must be finite in order to obtain reliable values of the SNR within reasonable time. This sets the lower border $q_0 \geq 2q_1$ for the range of q_0 and for the scale of the fractal structures for which the “fractal spectroscopy” by noise-free SMR can be used.

Going to the SR at higher harmonics we observe that the effect of collision of fractal structures of small scale, smaller than $2q_1$, can be still visible as clear maxima in the SNR, though it almost completely disappeared in the SNR at the fundamental frequency (cf. the discussion of Figs. 7(d) and 7(e) and 8(d) and 8(e) in Sec. 4.2, and of the object a in Figs. 4(a)–4(c) in Sec. 4.3). In this sense, SR at higher harmonics is a more sensitive tool for “fractal spectroscopy” with a finite periodic signal amplitude, able to detect collisions of fractal objects at a smaller scale. However, the curves SNR^(j) for $j > 1$ can contain many maxima separated by dips, connected with the collision of a single branch of the chaotic saddle with a single stripe of the basin (Sec. 4.2), which makes them hard to interpret. In practice, it is difficult to retrieve information on the model parameters in Eqs. (3) and (4) from the SNR at higher harmonics of the fundamental frequency.

6. Summary and Conclusions

In this paper we investigated numerically and theoretically noise-free SR at the fundamental frequency and its higher harmonics in chaotic systems close to crisis, in which the oscillations of the mean transient time versus the control parameter are observed. As models we used two-dimensional chaotic maps: the Hénon map and the kicked spin model. These models were analyzed as TC systems in which the escape events from the precritical attractor were treated as TC events. The curves of the SNR at the external periodic signal frequency versus the control parameter exhibited multiple maxima which is a signature of the noise-free SMR effect. The curves of the SNR at higher harmonics of the fundamental frequency were shown to possess even a more complicated structure consisting of many maxima and dips whose origin was explained using a model of the fractal chaotic saddle and the basin of escape colliding at the crisis point. The analogy with TC systems enabled us to show that our model systems

belong to a more general class of TC systems with a nonmonotonic derivative of the TC probability with respect to some control parameter, in which SMR appears if the periodic signal is added to this parameter. Finally, we discussed the possibility to measure macroscopic and experimentally observable quantities, including the SNR used typically to characterize SR, to retrieve information on the local (in the collision region) fractal structure of the chaotic saddles and basins of escape colliding at the crisis point. We coined the term “fractal spectroscopy” for this kind of indirect measurements.

When extending the previous studies of noise-free SMR to the case of SMR at higher harmonics, certain correspondence rules between the maxima and dips of the SNR at subsequent harmonics were derived. It was shown that the dips of the SNR at a higher harmonic, i.e. points where the SNR is equal to zero, correspond to broad, smooth maxima of the SNR at a lower harmonic. In the model systems close to crisis this happens in general far from the crisis point, where the broad maxima of the SNR at the fundamental frequency correspond to wide normal or anomalous oscillations of the mean escape time. On the other hand, sharp peaks of the SNR at the fundamental frequency and its higher harmonics can appear at the same value of the control parameter. This happens, in general, in systems with a distinct fractal structure of the basin of escape, when fractal structures collide whose scale (the largest relevant distance) is smaller than, approximately, twice the periodic signal amplitude. The above-mentioned correspondence rules are modification and extension to the case of noise-free SMR of the rules reported in [Loerincz *et al.*, 1999] for SR in TC systems with external noise.

Since SMR should be ubiquitous in systems in which the derivative of the TC probability depends on the control parameter in a nonmonotonic way, we expect that complicated curves of the SNR at higher harmonics of the fundamental frequency can also be often observed, with properties analogous to those obtained from our models. The complex shape of the TC probability may have all sorts of other reasons apart from the overlap of fractal sets, as in our examples. They may include, e.g. periodic windows, interplay of chaotic dynamics and external noise, etc. Whatever the reason, this would always lead to multiple maxima of the SNR at the fundamental frequency and higher harmonics. In particular, there are examples of experimental systems

with crises and probably fractal-induced oscillations of the mean escape time [Sommerer & Grebogi, 1992]. We briefly discussed the applicability of various kinds of “fractal spectroscopy” to characterize the local fractal properties of the sets colliding at the crisis point in such systems. When going from the method based on the measurement of the oscillations of the mean escape time to the SNR at the fundamental frequency to the SNR at its higher harmonics, the effect of the fractal structures becomes more spectacular: small oscillations of the mean escape time are turned into maxima of the SNR. Even small details of the fractal structure are clearly reflected in the large changes of the SNR with the rise of the control parameter. This is, however, at the expense of the increasing complexity of the curves SNR versus the control parameter which makes the interpretation of results difficult. Also the scale of the fractal structures which can be investigated by the “fractal spectroscopy” via the noise-free SMR is constrained by the amplitude of the periodic signal, which must be high enough to obtain reliable results.

Acknowledgments

This work was supported by the Polish Committee for Scientific Research under grant No. 5 P03B 007 21. S. Matyjaśkiewicz acknowledges the support of the DAAD scholarship for the stay at the Institute of Physics, Humboldt University at Berlin.

References

- Anishchenko, V. S., Neiman, A. B. & Safanova, M. A. [1993] “Stochastic resonance in chaotic systems,” *J. Stat. Phys.* **70**, 183–196.
- Anishchenko, V. S., Safanova, M. A. & Chua, L. O. [1994] “Stochastic resonance in Chua’s circuit driven by amplitude or frequency modulated signal,” *Int. J. Bifurcation and Chaos* **4**, 441–446.
- Anishchenko, V. S., Neiman, A. B., Moss, F. & Schimansky-Geier, L. [1999] “Stochastic resonance: Noise-enhanced order,” *Physics — Uspekhi* **42**, 7–36; *Usp. Fiz. Nauk* **169**, 7–38.
- Arai, K., Yoshimura, K. & Mizutani, S. [2002] “Dynamical origin of deterministic stochastic resonance,” *Phys. Rev.* **E65**, 015202 1–4.
- Bartussek, R., Hänggi, P. & Jung, P. [1994] “Stochastic resonance in optical bistable systems,” *Phys. Rev.* **E49**, 3930–3939.
- Bartussek, R., Jung, P. & Hänggi, P. [1995] “Stochastic resonance in optical bistable systems: Amplification and generation of higher harmonics,” *Chaos Solit. Fract.* **5**, 1775–1778.
- Benzi, R., Sutera, A. & Vulpiani, A. [1981] “The mechanism of stochastic resonance,” *J. Phys.* **A14**, L453–L457.
- Bulsara, A. R., Inchiosa, M. E. & Gammaitoni, L. [1996] “Noise-controlled resonance behavior in nonlinear dynamical systems with broken symmetry,” *Phys. Rev. Lett.* **77**, 2162–2165.
- Carroll, T. L. & Peccora, L. M. [1993] “Stochastic resonance and crises,” *Phys. Rev. Lett.* **70**, 576–579.
- Chapeau-Blondeau, F. [1995] “Stochastic resonance in the Heaviside nonlinearity with white noise and arbitrary periodic signal,” *Phys. Rev.* **E53**, 5469–5472.
- Chapeau-Blondeau, F. & Godivier, X. [1997] “Theory of stochastic resonance in signal transmission by static nonlinear systems,” *Phys. Rev.* **E55**, 1478–1495.
- Chizhevsky, V. N., Vilaseca, R. & Corbalán, R. [2000] “Amplification of non-resonant signals via stochastic resonance in a chaotic CO₂ laser,” *Phys. Rev.* **E61**, 6500–6505.
- Crisanti, A., Falcioni, M., Paladin, G. & Vulpiani, A. [1994] “Stochastic resonance in deterministic chaotic systems,” *J. Phys.* **A27**, L597–L603.
- Gammaitoni, L., Hänggi, P., Jung, P. & Marchesoni, F. [1998] “Stochastic resonance,” *Rev. Mod. Phys.* **70**, 223–287.
- Gingl, Z., Kiss, L. B. & Moss, F. [1995] “Non-dynamical stochastic resonance: Theory and experiments with white and arbitrarily coloured noise,” *Europhys. Lett.* **29**, 191–196.
- Ginzburg, S. L. & Pustovoit, M. A. [1999] “Stochastic resonance, on-off intermittency and ‘physical mathematics’,” *Europhys. Lett.* **45**, 540–544.
- Grebogi, C., Ott, E. & Yorke, J. A. [1986] “Critical exponents of chaotic transients in nonlinear dynamical systems,” *Phys. Rev. Lett.* **57**, 1284–1287.
- Grebogi, C., Ott, E., Romeiras, F. & Yorke, J. A. [1987] “Critical exponents for crisis-induced intermittency,” *Phys. Rev.* **A36**, 5365–5380.
- Grifoni, M. & Hänggi, P. [1996] “Coherent and incoherent quantum stochastic resonance,” *Phys. Rev. Lett.* **76**, 1611–1614.
- Grigorenko, A. N., Nikitin, S. I. & Roschepkin, G. V. [1997] “Stochastic resonance at higher harmonics in monostable systems,” *Phys. Rev.* **E56**, R4907–R4910.
- Hołyst, J. A. & Sukiennicki, A. [1992a] “Regular and chaotic behavior of a kicked damped spin,” *Acta Phys. Polonica* **A81**, 353–360.
- Hołyst, J. A. & Sukiennicki, A. [1992b] “Chaotic dynamics of a damped classical spin,” *J. Magn. Magn. Mater.* **104–107**, 2111–2112.
- Horita, T., Kanamaru, T. & Akishita, T. [1999] “Stochastic resonance-like behavior in the sine-circle map,” *Prog. Theor. Phys.* **102**, 1057–1064.
- Hou, Z., Yang, L. & Xin, H. [1999] “Stochastic bi-resonance without external signal in the CO + O₂

- catalytic oxidation reaction system," *J. Chem. Phys.* **111**, 1592–1594.
- Jung, P. [1993] "Periodically driven stochastic systems," *Phys. Rep.* **234**, 175–295.
- Jung, P. & Hänggi, P. [1991] "Amplification of small signals via stochastic resonance," *Phys. Rev.* **A44**, 8032–8042.
- Jung, P. & Talkner, P. [1995] "Suppression of higher harmonics at noise induced resonances," *Phys. Rev.* **E51**, 2640–2643.
- Kacperski, K. & Hołyst, J. A. [1997] "Control of crisis-induced intermittency in the dynamics of a kicked, damped spin," *Phys. Rev.* **E55**, 5044–5049.
- Kacperski, K. & Hołyst, J. A. [1999a] "Anomalous oscillations of average transient lifetimes near crises," *Phys. Lett.* **A254**, 53–58.
- Kacperski, K. & Hołyst, J. A. [1999b] "Theory of oscillations in average crisis-induced transient lifetimes," *Phys. Rev.* **E60**, 403–407.
- Kovaleva, A. & Simiu, E. [2000] "Chaotic resonance: Hopping rates, spectra and signal-to-noise ratios," *AIP. Conf. Proc.*, Vol. 502, pp. 428–433.
- Krawiecki, A. [1997] "Stochastic resonance in system with on-off intermittency," *Acta Phys. Polonica* **A92**, 1101–1108.
- Krawiecki, A., Matyjaśkiewicz, S., Kacperski, K. & Hołyst, J. A. [2001] "Noise-free stochastic multiresonance near chaotic crises," *Phys. Rev.* **E64**, 041104 1–4.
- Lindner, B. & Schimansky-Geier, L. [2001] "Transmission of noise coded versus additive signals through a neuronal ensemble," *Phys. Rev. Lett.* **86**, 2934–2937.
- Loerincz, K., Gingl, Z., Kiss, L. B. & Bulsara, A. R. [1999] "Higher order stochastic resonance in a level-crossing detector," *Phys. Lett.* **A254**, 154–157.
- Matyjaśkiewicz, S., Krawiecki, A., Hołyst, J. A., Kacperski, K. & Ebeling, W. [2001] "Stochastic multiresonance in a chaotic map with fractal basins of attraction," *Phys. Rev.* **E63**, 026215 1–10.
- McNamara, B. & Wiesenfeld, K. [1989] "Theory of stochastic resonance," *Phys. Rev.* **A39**, 4854–4869.
- Moss, F. [1994] "Stochastic resonance: From ice ages to monkey's ear," in *Contemporary Problems in Statistical Physics*, ed. Weiss, G. H. (SIAM, Philadelphia), pp. 205–253.
- Moss, F., Pierson, D. & O'Gorman, D. [1994] "Stochastic resonance: Tutorial and update," *Int. J. Bifurcation and Chaos* **6**, 1383–1397.
- Moss, F. [2000] "Stochastic resonance: Looking forward," in *Self-Organized Biological Dynamics & Nonlinear Control*, ed. Walleczek, J. (Cambridge University Press, Cambridge, UK), pp. 236–256.
- Nicolis, G., Nicolis, C. & McKernan, D. [1993] "Stochastic resonance in chaotic dynamics," *J. Stat. Phys.* **70**, 125–139.
- Nishimura, H., Katada, N. & Aihara, K. [2000] "Coherent response in a chaotic neural network," *Neural Proc. Lett.* **12**, 49–58.
- Pisarchik, A. N. & Corbalán, R. [1998] "Stochastic resonance in a chaotic laser," *Phys. Rev.* **E58**, R2697–R2700.
- Reibold, E., Just, W., Becker, J. & Benner, H. [1997] "Stochastic resonance in chaotic spin-wave dynamics," *Phys. Rev. Lett.* **78**, 3101–3104.
- Shiau, Y.-H. & Néda, Z. [2001] "A novel resonance in n-GaAs diodes," *Japanese J. Appl. Phys.* **40**, 6675–6676.
- Shneidman, V. A., Jung, P. & Hänggi, P. [1994] "Weak-noise limit of stochastic resonance," *Phys. Rev. Lett.* **72**, 2682–2685.
- Sinha, S. [1999] "Noise-free stochastic resonance in simple chaotic systems," *Physica* **A270**, 204–214.
- Sinha, S. & Chakrabarti, B. K. [1998] "Deterministic stochastic resonance in a piecewise linear chaotic map," *Phys. Rev.* **E58**, 8009–8012.
- Sommerer, J. C. & Grebogi, C. [1992] "Determination of crisis parameter values by direct observation of manifold tangencies," *Int. J. Bifurcation and Chaos* **2**, 383–396.
- Tsindlekht, M. I., Felner, I., Gitterman, M. & Shapiro, B. Ya. [2000] "Stochastic resonance phenomenon in a superconducting surface state of single-crystal Nb," *Phys. Rev.* **B62**, 4073–4078.
- Vilar, J. M. G. & Rubí, J. M. [1997] "Stochastic multiresonance," *Phys. Rev. Lett.* **78**, 2882–2885.
- Vilar, J. M. G. & Rubí, J. M. [1999] "Scaling concepts in periodically modulated noisy systems," *Physica* **A264**, 1–19.
- Wang, W. & Wang, Z. D. [1997] "Internal-noise-enhanced signal transduction in neuronal systems," *Phys. Rev.* **E55**, 7379–7384.
- Wiesenfeld, K., Pierson, D., Pantazelou, E., Dames, Ch. & Moss, F. [1994] "Stochastic resonance on a circle," *Phys. Rev. Lett.* **72**, 2125–2129.
- Wiesenfeld, K. & Moss, F. [1995] "Stochastic resonance and the benefits of noise: From the Ice Ages to crayfish and SQUIDS," *Nature* **373**, 33–36.
- Yuqing, W., Wang, Z. D. & Wang, W. [2000] "Dynamical behaviors of periodically forced Hindmarsh–Rose neural model," *J. Phys. Soc. Japan* **69**, 276–283.
- Zhang J.-Q. & Xin, H.-W. [2001] "Stochastic multiresonance induced by an optimal noise pulse interval due to hopping of energy levels," *Chinese Phys. Lett.* **18**, 870–873.
- Zhou, Ch. & Lai, C.-H. [1999a] "Amplification of weak signals and stochastic resonance in on-off intermittency with symmetry breaking," *Phys. Rev.* **E60**, 3928–3935.
- Zhou, Ch. & Lai, C.-H. [1999b] "Robustness of super-sensitivity to small signals in nonlinear dynamical systems," *Phys. Rev.* **E59**, R6243–R6246.

Appendix A The Explicit Form of the Spin Map

The explicit equations for the kicked spin map were derived in [Hołyst & Sukiennicki, 1992a, 1992b]. The map T_A can be written as

$$T_A \begin{bmatrix} \phi \\ S_z \end{bmatrix} = \begin{bmatrix} \phi + \Delta\phi \\ WS_z \end{bmatrix}, \quad (\text{A.1})$$

where ϕ is the angle between the x axis and the projection of the spin on the x - y plane,

$$\Delta\phi = (1/\lambda) \ln[(1 + S/S_z)/(1 + S/(WS_z))] - 2AS\tilde{\tau},$$

and $W = [c^2 + (S_z/S)^2(1 - c^2)]^{-1/2}$, $c = \exp(-2\lambda AS\tilde{\tau})$.

The map T_B can be written as

$$T_B \begin{bmatrix} \Phi \\ S_x \end{bmatrix} = \begin{bmatrix} \Phi - B \\ S - 2S(S - S_x)D^2U \end{bmatrix}, \quad (\text{A.2})$$

where Φ is the angle between the y axis and the projection of the spin on the x - z plane, $D = \exp(-\lambda B)$ and $U = [S + S_x + D^2(S - S_x)]^{-1}$.

Appendix B Evaluation of the Functions in the Analytic Formulae for the SNR

The expressions for the coefficients $\bar{\mu}_{kl}$ and $M_{kl,j}$ in Eq. (6), resulting from the overlap of the segment \mathcal{A}_k with the stripe \mathcal{B}_k , can be obtained as combinations of analogous coefficients resulting from the time-dependent overlap of the parabolic segment \mathcal{A}_k with a half-plane $y > c$, $c = \text{const}$. Introducing the continuous time approximation, the measure $\mu_k[c, t]$ of the latter overlap for small distance between the top of the parabola and the border of the plane, $q_0 + q_1 \cos \omega_0 t - (1 - \delta_{k,K+1})a\alpha^k - c \ll 1$, can be approximated as

$$\begin{aligned} \mu_k[c, t] &= \tilde{\mu}_k \sqrt{q_0 + q_1 \cos \omega_0 t - (1 - \delta_{k,K+1})a\alpha^k - c} \\ &\times \Theta[q_0 + q_1 \cos \omega_0 t - a(1 - \delta_{k,K+1})\alpha^k - c], \end{aligned} \quad (\text{B.1})$$

where $\Theta(\cdot)$ is the Heaviside step function. It follows that $\mu_k[c, t]$ is an even, periodic function of t . Following the notation of [Matyjaśkiewicz *et al.*, 2001] let us introduce the quantities

$$m_k(c) = \sqrt{2q_1/[q_0 - (1 - \delta_{k,K+1})a\alpha^k + q_1 - c]}, \quad (\text{B.2})$$

$$t_k(c) = \begin{cases} \omega_0^{-1} \arccos\{[c - q_0 + (1 - \delta_{k,K+1})a\alpha^k]/q_1\} & \text{if } q_{0,\min} \leq q_0 \leq q_{0,\text{full}}, \\ T_0/2 & \text{if } q_0 > q_{0,\text{full}} \end{cases} \quad (\text{B.3})$$

where $q_{0,\min} = c + (1 - \delta_{k,K+1})a\alpha^k - q_1$ and $q_{0,\text{full}} = c + a(1 - \delta_{k,K+1})\alpha^k + q_1$. The time $t_k(c)$ in Eq. (B.3) is defined so that \mathcal{A}_k overlaps the half-plane $y > c$ for $0 \leq t < t_k(c)$ and $T_0 - t_k(c) < t \leq T_0$; the overlap is nonzero during at least part of the period T_0 if $q_0 > q_{0,\min}$, and it is nonzero during the whole period if $q_0 > q_{0,\text{full}}$. Using this notation the time average $\bar{\mu}_k(c)$ and the j th Fourier coefficients $M_{k,j}(c)$, $j = 1, 2, 3$, of the function $\mu_k[c, t]$ can be evaluated as

$$\begin{aligned} \bar{\mu}_k(c) &= \frac{1}{T_0} \int_0^{T_0} \mu_k[c, t] dt \\ &= \frac{2\tilde{\mu}_k}{\pi} \sqrt{q_0 + q_1 - (1 - \delta_{k,K+1})a\alpha^k - c} E \left[\frac{\omega_0}{2} t_k(c), m_k(c) \right] \\ &\times \Theta[q_0 + q_1 - (1 - \delta_{k,K+1})a\alpha^k - c] \end{aligned} \quad (\text{B.4})$$

$$\begin{aligned} M_{k,j}(c) &= \frac{1}{T_0} \int_0^{T_0} \mu_k[c, t] \cos(j\omega_0 t) dt \\ &= \frac{2\tilde{\mu}_k}{\pi} \sqrt{q_0 + q_1 - (1 - \delta_{k,K+1})a\alpha^k - c} \end{aligned} \quad (\text{B.5})$$

$$\begin{aligned} & \times \left\{ Q_{k,j}(c) E \left[\frac{\omega_0}{2} t_k(c), m_k(c) \right] - R_{k,j}(c) F \left[\frac{\omega_0}{2} t_k(c), m_k(c) \right] \right\} \\ & \times \Theta[q_0 + q_1 - (1 - \delta_{k,K+1}) a \alpha^k - c] \end{aligned}$$

where $F(\phi, m) = \int_0^\phi (1 - m^2 \sin^2 x)^{-1/2} dx$ and $E(\phi, m) = \int_0^\phi (1 - m^2 \sin^2 x)^{1/2} dx$ are the elliptic integrals of the first and second kind, respectively, and

$$\begin{aligned} Q_{k,1}(c) &= \frac{2 - m_k^2(c)}{3m_k^2(c)}, \\ R_{k,1}(c) &= \frac{2 - 2m_k^2(c)}{3m_k^2(c)}, \\ Q_{k,2}(c) &= \frac{-16 + 16m_k^2(c) - m_k^4(c)}{15m_k^4(c)}, \\ R_{k,2}(c) &= \frac{16 - 24m_k^2(c) + 8m_k^4(c)}{15m_k^4(c)}, \\ Q_{k,3}(c) &= \frac{256 - 384m_k^2(c) + 134m_k^4(c) - 3m_k^6(c)}{105m_k^6(c)}, \\ R_{k,3}(c) &= \frac{-256 + 512m_k^2(c) - 310m_k^4(c) + 54m_k^6(c)}{105m_k^6(c)}. \end{aligned} \tag{B.6}$$

Thus the coefficients in Eq. (6) become

$$\begin{aligned} \bar{\mu}_{kl} &= \bar{\mu}_k [(1 - \delta_{l,L+1})(\beta^l b - \beta^l b_E)] - \bar{\mu}_k(\beta^l b), \\ M_{kl,j} &= M_{k,j} [(1 - \delta_{l,L+1})(\beta^l b - \beta^l b_E)] - M_{k,j}(\beta^l b). \end{aligned} \tag{B.7}$$

It follows that in the adiabatic approximation the SNR at all harmonics is independent of the periodic signal frequency ω_0 .

Copyright of International Journal of Bifurcation & Chaos in Applied Sciences & Engineering is the property of World Scientific Publishing Company and its content may not be copied or emailed to multiple sites or posted to a listserv without the copyright holder's express written permission. However, users may print, download, or email articles for individual use.